Optimization of a Seeded Free-Electron Laser with Helical Undulators

M. Labat, M. Hosaka, M. Shimada, M. Katoh, and M. E. Couprie*

Centre CEA-Saclay, DSM/DRECAM/SPAM, 91 191 Gif-sur-Yvette, France
Nagoya University, Furo-cho, Chikusa-ku, Nagoya 464-8603, Japan
UVSOR, Institute for Molecular Science, Myodaiji, Okazaki 444, Japan
Synchrotron SOLEIL, Saint Aubin, B.P. 34, 91 192 Gif-sur-Yvette, France

(Received 11 April 2008; published 17 October 2008)

Seeded single pass free-electron lasers are promising coherent, short-duration, and intense light sources, from the visible to x rays. Operated with adjustable undulators, they are also a unique device for providing fully variable polarized radiation. We report here the first seeding of helical undulators with a variable polarized source. We demonstrate that the adjustment of the seed polarization and focusing allows the free-electron laser radiation to be optimized in terms of intensity and quality.

DOI: 10.1103/PhysRevLett.101.164803 PACS numbers: 41.60.Cr, 42.25.Ja, 42.65.Ky

Electronic and structural properties of matter are often investigated using short wavelength coherent pulsed radiation. Users select the light source according to the required properties, such as pulse duration, coherence, or polarization. X-ray lasers produce discrete spectral line radiation down to 5.8 nm [1] with a limited spatial coherence [2]. High order harmonics can be generated by focusing an intense laser on rare gas [3] or on solid targets [4], providing tunable coherent radiation down to the water window [5,6] with a pulse duration reaching the attosecond range [7]. Because of the involved intrinsic physical process, such sources cannot give a fully adjustable polarization [8–10]. A postconversion scheme can be applied to radiation down to 120 nm according to the further developments on optics for shorter wavelengths based on multilayer systems [11]. Accelerator-based bending magnet synchrotron radiation offered the first tunable polarization source. Then the advent of various magnetic schemes of undulators [12–15] on third-generation synchrotron sources enabled the delivery of intense, spatially coherent synchrotron radiation pulses down to x rays with high repetition rate variable polarization. The free-electron lasers (FELs), based on the amplification, along an undulator, of an optical wave in a relativistic electron beam, lead to similar polarization flexibility [16,17] together with shorter duration and higher intensity pulses. The self-amplified spontaneous emission (SASE) FEL [18], starting from noise, has a limited temporal coherence, due to the absence of correlation of the different radiation trains. The coherent harmonic generation (CHG) FEL is an improved alternative, using an external laser source [19–21] or high harmonics in gas [22] for seeding which correlates the trains. In both low and high gain regimes, the interaction of the electrons with the external source injected inside a first undulator (called the modulator) tuned to the laser wavelength induces an energy modulation. This modulation is converted in a dispersive section (or a drift space) into a density modulation which leads to coherent emission in a second undulator (called the radiator). The FEL reproduces the coherence of the injected source, and its polarization is determined by the magnetic arrangement of the radiator: Planar to helical undulators drive linear to circular polarizations.

Operated with adjustable undulators, the CHG FEL finally appears as a unique candidate for providing really flexible polarized light of high quality. Thus, based on the same interaction process, low gain CHG FELs usually require high seeding power and are limited to the vacuum ultraviolet range while high gain devices, thanks to a strong exponential growth, can radiate down to the soft-x-ray range, required for probing symmetry properties of matter [23–25]. Experiments are already foreseen on the future high gain FEL devices aiming at delivering subpicosecond subnanometer pulses with variable polarization such as BESSY-FEL [26] and FERMI [27]. CHG has been performed using linear polarized lasers for seeding both planar and helical undulators [28,29]. In this Letter, we report on the first optimization of a seeding source for helical undulators. We show that the FEL radiation properties can be significantly improved via the adjustment of the seed polarization and focusing. The measured FEL behaviors are understood using a simple 1D analytical model and further confirmed using the 3D numerical code GENESIS [30].

The experiments were performed on the CHG FEL of the UVSOR-II storage ring [28] (Okazaki, Japan). A basic scheme of the setup is presented in Fig. 1. The modulator, the radiator, and the dispersive section are combined in a single structure called an optical klystron [31]. Each element consists of magnet arrays assembled in three lanes, creating vertical and horizontal magnetic fields. The shifting of the lanes changes the phase between the vertical and horizontal components and tunes the total magnetic field from planar to helical [32], driving the radiation polarization from linear to circular. Here, the optical klystron is set in the helical configuration. A femtosecond laser system at 800 nm is focused inside the optical klystron with two possible Rayleigh length Z_R values. This setup enables us to study the influence of the seed focusing on the harmonic generation process. A quarter-wavelength plate on the laser

 © 2008 The American Physical Society

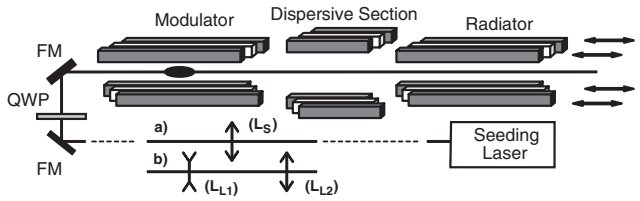

FIG. 1. Schematic of a CHG FEL in helical configuration. UVSOR-II electron beam: normalized energy $\gamma = 978$; relative energy spread $\sigma_\gamma = 2.8 \times 10^{-4}$. Modulator and radiator: 9 periods of 11 cm with a deflection parameter 3.8. Dispersive section: $N_d = 70$ equivalent periods. Seeding laser: Ti:sapphire system (Coherent) delivering 1 ps-FWHM, 2.5 mJ pulses at 1 kHz with focusing configuration: (a) $Z_R = 0.15$ m with (L_S) a 5 m focusing lens (waist: 200 μm); (b) $Z_R = 1.5$ m with (L_{L1}) a 1 m focusing lens and (L_{L2}) a 0.5 m defocusing lens (waist: 600 μm). Waist position: at the end of the modulator. QWP: quarter-wavelength plate. FM: flat mirrors.

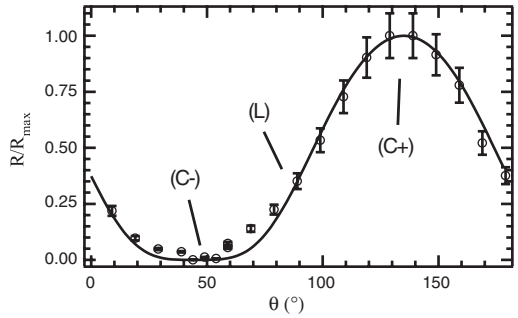

FIG. 2. $R/R_{\max}$ of the second coherent harmonic versus the angle of the QWP. (○) Experimental data with error bars of 10% corresponding to the intensity fluctuation mainly due to the laser transport [measurement with a photomultiplier (R928, Hamamatsu)]. Line: Calculation using Eq. (5). $P_L = 0.84$ W, $\sigma_L = 425$ fs, $Z_R = 1.5$ m. $f_{\text{det}} = \frac{\sigma_L}{\sigma_e}\frac{\Delta\lambda_{\text{Las}}}{\Delta\lambda_{\text{SE}}} = 3.16 \times 10^{-4}$, $\sigma_e =$ 90 ps rms, the bunch length, $\Delta\lambda_{\text{Las}} = 1.5$ nm (respectively, $\Delta\lambda_{\text{SE}} = 22$ nm) the spectral width of the coherent harmonic (respectively, spontaneous emission). (L): linear; (C+/−): circular polarization.

beam gradually tunes the seeding laser polarization from linear to circular for the CHG optimization with the seeding laser polarization. When the seeding laser and the electron beam overlap temporally, second and third harmonics are generated (respectively, at 400 and 266 nm), exhibiting clear enhancement with respect to the spontaneous emission, due to the additional coherent photons. The measured efficiency of the harmonic generation is evaluated using the ratio $R =$ (coherent emission)/(spontaneous emission).

Circles (○) in Fig. 2 show the intensity of the coherent second harmonic as a function of the quarter-wavelength plate angle θ (between incident linear polarization and the phase plate ordinary axis), i.e., of the seeding laser polarization. When the angle is set to $\theta = 0°$, the laser keeps its initial linear polarization. Second-harmonic generation is thus performed with a low efficiency ($R = 0.2$). The intensity reaches a maximum for a circular polarization of the laser (C +, $\theta = 135°$) ($R \approx 0.8$). For a circular polarization in the opposite direction (C −, $\theta = 45°$), the coherent emission vanishes. For an elliptical polarization of the seeding laser (intermediate θ), the coherent harmonic intensity remains below the maximum. This behavior can be interpreted using a 1D analytical model as follows.

Within an undulator in helical configuration, the electron beam describes a helix around the magnetic axis at the normalized velocity $\vec{\beta}_e$. The helix turns in a direction (+) opposite to the helical magnetic field direction. At the waist position, the seeding laser electric field $\vec{E}_L$ at frequency $\omega_L = k_L c$ propagating in the z direction is

$$\vec{E}_L = |\vec{E}_L|[\sin(\theta)\cos(k_L z - \omega_L t)\vec{e}_x + \cos(\theta)\sin(k_L z - \omega_L t)\vec{e}_y], \quad (1)$$

with a polarization angle θ and an amplitude

$$|\vec{E}_L| \propto [P_L e^{-t^2/2\sigma_L^2} f_{\text{rep}}^{-1} \sigma_L^{-1} Z_R^{-1}]^{1/2}. \quad (2)$$

which depends on its average power P_L, repetition rate f_{rep}, and Rayleigh length Z_R. The term $e^{-t^2/2\sigma_L^2}$ represents the Gaussian intensity profile in the time domain (t), with rms pulse duration σ_L [i.e., FWHM $= 2\sqrt{2\ln(2)}\sigma_L$]. With $\theta = 135°$, the polarization turns in the (+) direction and with $\theta = 45°$ in the opposite (−) direction. Along the modulator, the electrons and the seeded laser exchange an energy:

$$\delta\gamma = -\frac{e}{mc}\int_{L_{\text{mod}}} \vec{E}_L(\theta)\cdot\vec{\beta}_e dt, \quad (3)$$

which is maximum for $\theta = 135°$, i.e., when the polarization of the laser is circular and turning in the same direction as the electron beam velocity, and null for $\theta = 45°$. The variation of the seeding polarization optimizes the coupling between the laser and the electron beam inside the modulator, enhancing the energy exchange. This energy exchange further drives an energy modulation of the electron beam with a maximum amplitude $\Delta\gamma$, converted into a phase modulation: $\Delta\alpha = 4\pi(N + N_d)\Delta\gamma/\gamma$, as the electron beam passes through the dispersive section. N and N_d [33] are the numbers of, respectively, the modulator and the equivalent dispersive section periods. The distribution is bunched at the seeding laser fundamental wavelength λ_L and its harmonics $\lambda_L/2$, $\lambda_L/3, \ldots$ with the bunching functions b_n:

$$b_n = f_n J_n(n\Delta\alpha), \quad (4)$$

with J_n standing for the Bessel function of order n and $f_n = e^{-8[n\pi(N+N_d)\sigma_\gamma]^2}$ for the modulation rate depending on the relative energy spread σ_γ. The ratio R_0 of coherent emission in the radiator integrated along the laser distribution is finally given by

$$R_0 = \int N_e C_n J_n^2(n\Delta\alpha)dt, \qquad R = f_{\text{det}} R_0. \quad (5)$$

N_e is the number of electrons contributing to the coherent emission, while C_n includes 3D effects [34]. The effect of the detector integration of the signal over time and spec-

trum is considered in the f_{det} factor (see Fig. 2). In agreement with the experimental results of Fig. 2, the ratio of coherent emission R calculated using Eq. (5) also leads to a maximum when the seeding laser polarization vector matches the electron beam velocity vector, i.e., when it is circular with the proper direction. Furthermore, coherent emission is canceled in the case of the opposite direction. We have demonstrated that, in the case of helical undulators, the intensity of the circular polarized coherent harmonic can be optimized with the seeding laser polarization. In addition, since both the seeding laser polarization (via the quarter-wavelength plate) and the undulator configuration (via the phase of the lanes) can be tuned, such a setup can be used to provide an optimized coherent light with a full variable polarization.

We then measured the intensity of the second harmonic versus θ for short Z_R and different seeding powers P_L as presented in Fig. 3. The increase of P_L leads to an enhancement of $\Delta\theta$, the FWHM of the plots. In addition, the top of the plot flattens. According to Eq. (5), the intensity ratio R depends on the laser power via the argument of the Bessel functions, proportional to the bunching function. The Bessel functions are not continuously increasing: They reach a maximum at $n\Delta\alpha = 1.89$. Once this optimum is passed, J_n and b_n decrease, corresponding to a degradation of the bunching, and, accordingly, R decreases. In the case of high seeding power, maximum energy exchange with matched polarization gives an $n\Delta\alpha$ beyond the optimum. A detuned polarization (slightly elliptical, for instance) reduces the energy exchange and avoids an overbunching of the electron beam and the subsequent decrease of R. In agreement with the experimental results, the new optimized polarizations are shifted towards elliptic cases, which enlarges and flattens the top of the plots. The analysis of the intensity variation versus θ in Fig. 3 reveals that overbunching is driven at high seeding power.

Additional measurements and analytical calculations of $\Delta\theta$ and R, for several P_L in the two focusing configurations, are given in Table I. The tendency presented in the example of Fig. 3 is fully confirmed: In both focusing conditions, the seeding power increase causes a net broadening of the plots. Discrepancies between experiments and model ($\Delta\theta_{\mathrm{expt}} > \Delta\theta_{\mathrm{model}}$) can result from the 1D approximation of the model, which does not completely take into account either the transverse dimensions of the beams or the evolution along the undulator. The seeding power increase also enables stronger coherent emission. The maximum ratio R is reached with maximum P_L, and the harmonic generation is more efficient using a short Z_R. The calculations predict similar evolution: A long Z_R favors the process in terms of number of photons, but the calculated stronger enhancement of the CHG and saturation beyond 0.4 W using the short Z_R could not be observed. In addition, with large P_L and long Z_R, $\Delta\theta$ is narrower than with the short Z_R, indicating that the distribution is less "debunched," i.e., degraded. The enhancement of the fluctuations from ≈10% using the long Z_R (see Fig. 2) to ≈30% using the short Z_R (see Fig. 3) reinforces the conclusion that the strong focusing may cause degradation of the radiation quality, here in terms of stability, and the bunching profile.

The focusing mode influence is verified with the 3D numerical code GENESIS [30], which takes into account the varying geometry of the interaction related to the laser and electron beam sizes evolution along the undulator. The laser beam size is defined by the Z_R and the electron beam size by the lattice functions. The simulations have been performed on the fundamental using a linear polarized seeding laser (imposed by the input field format), but the results can be applied to the case of a circular polarized seeding laser and for the higher harmonics. Indeed, according to Eq. (3) and to the results of Fig. 3, the circular polarization allows a more efficient energy exchange which can be compensated for a linear polarization by the use of a higher P_L, and, according to Eq. (4), the harmonic behavior is scaled to the fundamental's. Figures 4(a)–4(c) show bunching profiles b_1 on the fundamental for different Z_R using $P_L = 10$ MW. For $Z_R = 3$ m [Fig. 4(b)], the profile is smooth and Gaussian. For a longer Z_R [Fig. 4(c)], the profile is still Gaussian with a lower maximum value. For a shorter Z_R [Fig. 4(a)], the profile is concave with maxima

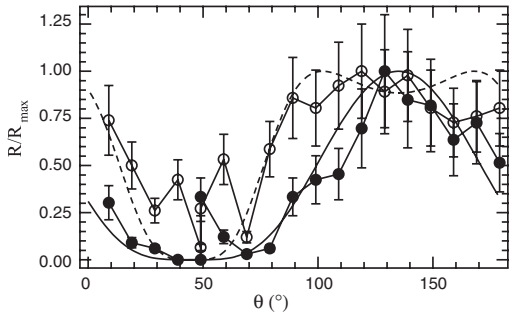

FIG. 3. R/R_{max} on the second harmonic versus θ. $\sigma_L = 425$ fs rms, $Z_R = 0.15$ m. (○, •) Experiment (with error bars of 30% corresponding to the intensity fluctuation mainly due to the laser transport) and (continuous line, dashed line) calculation [based on Eq. (5), $f_{\mathrm{det}} = 3.16 \times 10^{-4}$]. • and continuous line with $P_L = 0.05$ W, ○ and dashed line with $P_L = 0.32$ W.

TABLE I. Width $\Delta\theta$ and maximum R of the plots versus θ (see Fig. 2) for various P_L and Z_R. Expt: experiment, Theor: calculation using Eq. (5), $f_{\mathrm{det}} = 3.16 \times 10^{-4}$. $\Delta\gamma$ is reduced by factor 0.4 to take into account the seed laser transport losses and transverse overlap with the electron beam.

P_L (W)	Z_R (m)	$\Delta\theta$ (deg): Theor.|Expt.	R: Theor.|Expt.
0.05	0.15	68|68	0.20|0.54
0.13	0.15	78|136	0.74|0.74
0.32	0.15	116|140	1.08|0.86
0.55	0.15	132|147	1.08|1.05
0.84	1.5	73|73	0.50|0.82
1.48	1.5	84|128	0.91|1.26

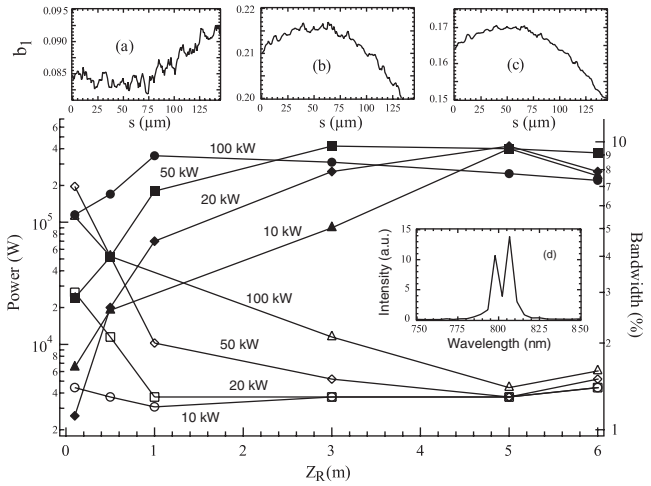

FIG. 4. GENESIS simulation of the UVSOR-II CHG FEL on the fundamental at the radiator exit. Peak power (solid marker) and FWHM spectral width (empty marker) vs Z_R. Insets: b_1 along the electronic distribution for (a) $Z_R = 0.1$ m, (b) $Z_R = 3$ m, and (c) $Z_R = 10$ m using $P_L = 10$ MW; (d) FEL spectrum on the fundamental using $Z_R = 2$ m and $P_L = 1$ GW. Other parameters are given in Fig. 1.

reached on the edges, revealing that the distribution is debunched. A short Z_R can lead to a degradation of the bunching profile as shown previously. The coherent output power on the fundamental as a function of Z_R exhibits an optimum which depends on P_L (see Fig. 4). The seeding power decrease can be compensated by a Z_R increase, which maintains the maximum available energy exchange [see Eq. (3)], i.e., the maximum available output coherent power. The influence of Z_R on the FEL temporal properties is estimated via the spectrum width on the fundamental, also plotted in Fig. 4. As for the output power, the FEL spectral width shows an optimum (a minimum) in Z_R. Using a strong power and a strong focusing mode can even, as a result of a strong debunching, generate substructures in the spectrum [see Fig. 4(d)]. Indeed, sidebands have been observed in the spectrum of an oscillator FEL [35] for high intracavity optical power and of a SASE FEL when "debunching" starts in the postsaturation regime [36]. According to these results, the CHG FEL can be optimized in terms of output intensity and temporal properties using Z_R.

In conclusion, we demonstrated that the seeded FEL on UVSOR-II can be optimized using the seeding laser polarization and focusing mode. The analysis of the polarization dependence reveals that overbunching driven by strong seeding power could be reduced by smoothing the seeding laser focusing. The experimental results are explained by both analytical model and 3D simulations. The results obtained here in the small-gain regime can be applied to any seeded FEL configurations, since all rely on a similar energy exchange initial step, which include the next generation CHG FELs, such as SPARC, SPARX [37], and FLASH [38], and, in particular, those aiming at delivering ≈10 fs pulses with *variable polarization* in the nanometer range such as BESSY and FERMI.

*marie.labat@synchrotron-soleil.fr

[1] R. Smith, Phys. Rev. A **59**, R47 (1999).
[2] M. A. Larotonda *et al.*, IEEE J. Sel. Top. Quantum Electron. **10**, 1363 (2004).
[3] P. Salieres *et al.*, Phys. Rev. Lett. **74**, 3776 (1995).
[4] S. Gordienko *et al.*, Phys. Rev. Lett. **94**, 103903 (2005).
[5] M. Zepf *et al.*, Phys. Rev. Lett. **99**, 143901 (2007).
[6] B. Dromey *et al.*, Phys. Rev. Lett. **99**, 085001 (2007).
[7] I. Christov *et al.*, Phys. Rev. Lett. **78**, 1251 (1997).
[8] K. Budil *et al.*, Phys. Rev. A **48**, R3437 (1993).
[9] P. Zeitoun *et al.*, Nature (London) **431**, 426 (2004).
[10] T. Kawachi *et al.*, Phys. Rev. Lett. **75**, 3826 (1995).
[11] F. Schafers, Physica (Amsterdam) **283B**, 119 (2000).
[12] P. Elleaume, Rev. Sci. Instrum. **60**, 1830 (1989).
[13] R. Walker and B. Diviacco, Rev. Sci. Instrum. **63**, 332 (1992).
[14] S. Sasaki, Nucl. Instrum. Methods Phys. Res., Sect. A **347**, 83 (1994).
[15] O. Marcouillé *et al.*, in *Proceedings of the 2007 Particle Accelerator Conference (PAC)* (IEEE, New York, 2007), pp. 929–931.
[16] G. Dattoli and L. Bucci, Opt. Commun. **177**, 323 (2000).
[17] Y. Wu *et al.*, Phys. Rev. Lett. **96**, 224801 (2006).
[18] A. M. Kondratenko and E. L. Saldin, Sov. Phys. Dokl. **24**, 986 (1979).
[19] A. Doyuran *et al.*, Phys. Rev. Lett. **86**, 5902 (2001).
[20] R. Prazeres *et al.*, Nucl. Instrum. Methods Phys. Res., Sect. A **272**, 68 (1988).
[21] L. Yu *et al.*, Phys. Rev. Lett. **91**, 074801 (2003).
[22] G. Lambert *et al.*, Nature Phys. **4**, 296 (2008).
[23] L. Young *et al.*, Phys. Rev. Lett. **97**, 083601 (2006).
[24] J. Vogel *et al.*, Appl. Phys. Lett. **82**, 2299 (2003).
[25] L. Nahon *et al.*, Appl. Opt. **43**, 1024 (2004).
[26] http://www.bessy.de/, 2008.
[27] http://www.elettra.trieste.it/FERMI/, 2008.
[28] M. Labat *et al.*, Eur. Phys. J. D **44**, 187 (2007).
[29] G. DeNinno *et al.* (to be published).
[30] S. Reiche, Nucl. Instrum. Methods Phys. Res., Sect. A **429**, 243 (1999).
[31] N. Vinokurov and A. Skrinsky, Nuclear Physics Institute of Novossibirsk Report No. 77-59, 1977.
[32] H. Hama, Nucl. Instrum. Methods Phys. Res., Sect. A **375**, 57 (1996).
[33] P. Elleaume, J. Phys. (Paris) **44**, C1 (1983).
[34] V. Litvinienko *et al.*, Nucl. Instrum. Methods Phys. Res., Sect. A **507**, 265 (2003).
[35] R. Warren *et al.*, Nucl. Instrum. Methods Phys. Res., Sect. A **285**, 1 (1989).
[36] A. Lumpkin *et al.*, Phys. Rev. Lett. **88**, 234801 (2002).
[37] C. Vaccarezza *et al.*, in *Proceedings of the PAC'07 Conference, Albuquerque, New Mexico* (Joint Accelerator Conferences Website, 2007), p. 1001.
[38] H. Schlarb, in *Proceedings of the FEL'07 Conference, Novosibirsk, Russia* (Joint Accelerator Conferences Website, 2007), p. 211.